

Probing Galaxy Formation with TeV Gamma Ray Absorption

Joel R. Primack ^{a,b} James S. Bullock ^a Rachel S. Somerville ^b
 Donn MacMinn ^c

^a*Physics Department, University of California, Santa Cruz, CA 95046 USA*

^b*Racah Institute of Physics, The Hebrew University, Jerusalem 91904, Israel*

^c*Deceased*

Abstract

We present here the extragalactic background light (EBL) predicted by semi-analytic models of galaxy formation, and show how measurements of the absorption of gamma rays of \sim TeV energies via pair production on the EBL can probe cosmology and the formation of galaxies. Semi-analytic models permit a physical treatment of the key processes of galaxy formation – including gravitational collapse and merging of dark matter halos, gas cooling and dissipation, star formation, supernova feedback and metal production – and have been shown to reproduce key observations at low and high redshift. Using this approach, we investigate the consequences of variations in input assumptions such as the stellar initial mass function and the underlying cosmology. We conclude that observational studies of the absorption of $\sim 10^{-2} - 10^2$ TeV gamma rays will help to constrain the star formation history of the universe, and the nature and extent of the extinction of starlight due to dust and reradiation of the absorbed energy at infrared wavelengths.

Key words: cosmology: observations, diffuse radiation – infrared: galaxies – galaxies: evolution – gamma rays: theory

1 Introduction

It has long been appreciated that high energy γ -rays from sources at cosmological distances will be absorbed via electron-positron pair production [1] on the diffuse background of long wavelength photons produced over the history of the universe. Now that several extragalactic TeV sources have been discovered, it is beginning to become possible to use this process to probe the extragalactic background light (EBL). This technique will become increasingly powerful as many more sources will presumably be discovered at greater

distances with the new generation of γ -ray telescopes (GLAST, CELESTE, STACEE, MAGIC, HESS, VERITAS, and Milagro).

Broadly speaking, there are three approaches to studying the EBL/ γ -absorption connection, represented by the three speakers on this topic here at the VERITAS workshop:

- Limits on the EBL, and on models for its production, from γ -absorption data [2];
- Semi-empirical estimates of the EBL [3]; and
- Prediction of the EBL and γ -absorption from physical theories of galaxy formation and evolution in a cosmological framework.

The advantage of the last of these approaches, which we will follow in this talk, is that it permits one to deduce from γ -ray absorption data a great deal about galaxy formation and evolution, including the effects of the stellar initial mass distribution and of dust extinction and reradiation. It is also arguably the best way to estimate the extent of γ -ray absorption at various energies, as shown by the correct prediction from a simplified model of this sort [4, hereafter MP96] that there would be rather little absorption of TeV γ -rays from the nearest extragalactic sources, Mrk 421 and Mrk 501, at redshifts of only $z = 0.03$. The calculations reported here (and in more detail in [5] and [6]) are based on state-of-the-art semi-analytic models (SAMs) of galaxy formation, which we summarize briefly below. But it will be useful to start by summarizing our earlier calculations (MP96).

2 Simplified Cosmological Modeling of the EBL

Although there is a long history of spectral synthesis models leading to predictions for the EBL (e.g., [7–9]), such models typically attempted to account only for the star formation history of the galaxies existing today — i.e., they are pure luminosity evolution models. Moreover in spectral synthesis, the star formation history of each galaxy is *not* determined from its cosmological history, taking into account the fact that gas is not available to form stars until it has cooled within a dense collapsed structure. But the evidence is certainly increasing that there was a great deal of galaxy formation and merging in the past, plausibly in agreement with the predictions of hierarchical models of galaxy formation of the CDM type.

The motivation of the approach used by MP96 was to obtain theoretical predictions for the EBL and the resulting absorption of γ -rays in the context of hierarchical theories of structure formation, specifically within the CDM family of cosmological models. It is relatively straightforward to calculate

the evolution of structure in the dark matter component within the CDM paradigm. In MP96, the number density of dark matter halos as a function of mass and redshift and its dependence on cosmology was modeled using Press-Schechter theory, which agrees fairly well with the predictions of N-body simulations. However, obtaining the corresponding radiation field as a function of time and wavelength involves complicated astrophysics with many unknown parameters. This problem was addressed empirically, using the simple assumption that each dark matter halo hosts one galaxy, with the galaxy luminosity assumed to be a monotonic function of the halo mass. To model the spectrum of each galaxy, the star formation rate (SFR) was assumed to be $\propto e^{-t/\tau}$, with ellipticals (assumed to be 28% of the galaxies) having $\tau = 0.5$ Gyr, and spirals (the remaining 72%) having $\tau = 6$ Gyr. The actual SFR for each galaxy was determined so that a desired local luminosity function (LLF) was reproduced at redshift $z = 0$. As there is considerable variation in the observed B-band luminosity function derived from different redshift surveys, MP96 considered three representative choices.

Stellar emission was modeled in a simplified way, with each stellar population of a given mass and age treated as a black body with the appropriate temperature. Three different power-law initial mass functions (IMFs) $N(M) \propto (M/M_\odot)^{-1+\Gamma}$ describing the differential distribution of the initial stellar masses were considered: the standard Salpeter IMF with $\Gamma = -1.35$, and also steeper IMFs with $\Gamma = -1.6$ and -2.0 . The evolution of the gas content and metallicity within each galaxy was treated in the instantaneous recycling approximation. Dust absorption was treated in a standard way [10], assuming that the mass of dust increases with the galaxy metallicity and gas fraction. The extinction curve was similar to a Galactic extinction curve, but was scaled according to the metallicity (galaxies with lower metallicities have steeper extinction curves in the UV, as indicated by observations of the LMC and SMC). Energy was conserved, so that any energy absorbed by dust was reradiated. The dust emission spectrum was modeled [11] with three components: PAH molecules (~ 10 to 30 μm), warm dust from active star forming regions (30 to 70 μm), and cold “cirrus” dust (70 to 1000 μm).

Two cosmological models were considered, a standard (cluster-normalized, $\sigma_8 = 0.67$) $\Omega_{\text{matter}} = 1$ cold dark matter (SCDM) model, and a COBE-normalized cold + hot dark matter (CHDM) model with the then-favored hot dark matter fraction $\Omega_\nu = 0.3$. Since both were $\Omega_{\text{matter}} = 1$ models, the Hubble parameter was chosen to be $h = 0.5$ ($H_0 = 100h \text{ km s}^{-1} \text{ Mpc}^{-1}$) in order to obtain a Universe with an age of 13 Gyr. Galaxy formation occurs fairly early in the SCDM model (because of the large amount of power on small scales), and considerably more recently in the CHDM model.

The main conclusion from this study was that cosmology is the dominant factor influencing the EBL in the range 1-10 μm , which is the range most

relevant for absorption of \sim TeV γ -rays from nearby extragalactic sources. In this wavelength range, the most extreme differences between the three different LLFs and three different IMFs considered were less than the difference between the SCDM and CHDM cosmological models, representing early and late galaxy formation respectively. It is not difficult to understand why this happens: since the optical luminosity at $z = 0$ was fixed for each assumed LLF, the main factor determining the EBL in the near infrared was the star formation history. Because galaxies were assumed to trace halos in a simple way, the star formation history was almost entirely determined by the cosmology. As MP96 explained, the SCDM model predicted a larger EBL flux because (1) the stars have put out more light since they have been shining longer than in CHDM, (2) there was more redshifting of their light from the optical to the near infrared, and (3) the SCDM galaxies are older at a given redshift and hence are composed of more evolved stars, producing more flux in the red and near-infrared.

As expected, when the optical depth for γ -rays due to e^+e^- production was calculated, more absorption was predicted for SCDM than for CHDM. But for sources as near as Mrk 421 and 501, the predicted absorption only steepens the spectrum a little in the 300 GeV - 10 TeV range for which results have thus far been published, with curvature noticeable mainly above about 3 TeV. These predictions appear to be consistent with the observations [12], unlike those from earlier [13] and later [14] calculations based on a semi-empirical approach. The predictions of our new, more complete treatment are qualitatively consistent with this earlier simplified approach.

3 Semi-Analytic Modeling of the EBL

Our new approach is based on semi-analytic models (SAMs) of galaxy formation, which allow one to model the astrophysical processes involved in galaxy formation in a simplified but physical way within the framework of the hierarchical structure formation paradigm. The semi-analytic models used here are described in detail in [15], [16], and [17]. These models are in reasonably good agreement with a broad range of local galaxy observations, including the relation between luminosity and circular velocity (the Tully-Fisher relation), the B-band luminosity function, cold gas contents, metallicities, and colors [16]. Our basic approach is similar in spirit to the models originally presented by [18] and [19], and subsequently developed by these groups in numerous other papers (reviewed in [15] and [16]). Significant improvements included in [16] are that we assumed a lower stellar mass-to-light ratio (in better agreement with observed values), included the effects of dust extinction, and developed an improved “disk-halo” model for supernovae feedback. With these new ingredients, we were able to overcome some of the difficulties of previous models,

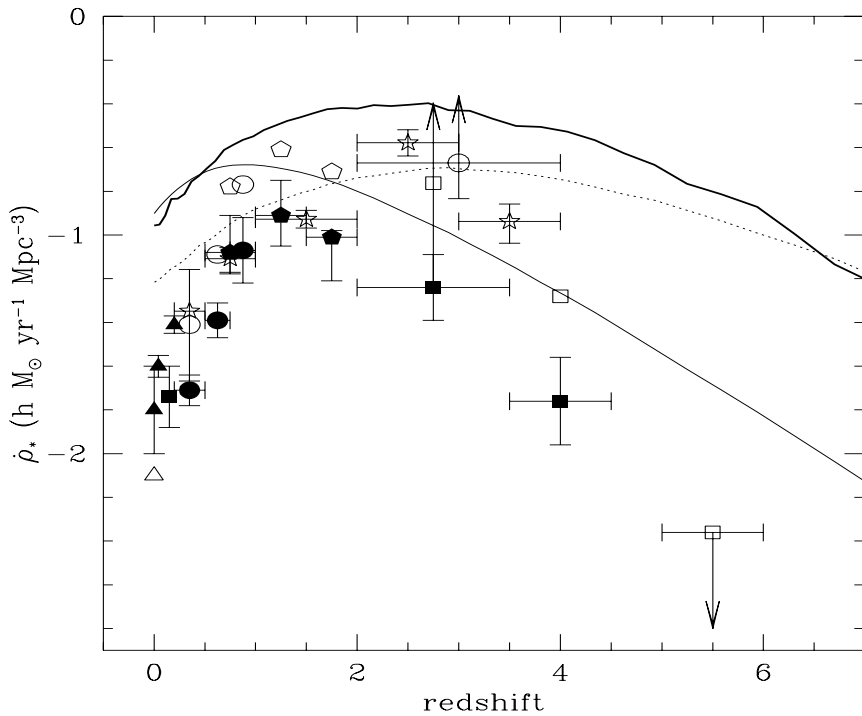


Fig. 1. The global star formation rate as a function of redshift, for three different SCDM models of star formation. The light solid line shows a model with constant star formation efficiency, including quiescent star formation only. The bold solid line assumes constant efficiency quiescent star formation, but contains a contribution from starbursts induced by galaxy-galaxy collisions [17]. The dotted line represents only quiescent star formation, but the efficiency of star formation is assumed to scale inversely with the dynamical time of the galaxy, therefore star formation is more efficient at high redshift because the typical objects are smaller and have shorter dynamical times. This model is similar to the fiducial model of Somerville & Primack [16], and to the models of Kauffmann et al. The data shown as filled symbols are uncorrected for extinction; the corresponding open symbols show the extinction correction suggested in [20]. The tip of the left vertical arrow shows a correction of a factor of seven, which may be indicated by recent observational studies of dust extinction in Lyman break galaxies. The large open circle at $z = 3$ shows the lower limit from the SCUBA observations of the HDF region [21] (assuming that these sources are stellar rather than AGN). (More complete descriptions of the data with references are given in [22].) Note that the discrepancy between the predictions and the data at low redshifts ($z \lesssim 1$) is partly alleviated when the models are corrected downward by about a factor of 2, to correct for the overprediction of the number density of $M \lesssim 0.1M_*$ halos in the Press-Schechter approximation.

which did not simultaneously reproduce the Tully-Fisher relation and B-band luminosity function, and produced bright galaxies that were too blue.

Instead of assuming a one-to-one relationship between galaxies and dark matter halos, as in MP96, we now determine the galaxy population residing in

halos of a given mass by constructing the “merging history” of each halo using an extension of the Press-Schechter technique. Using the method described in [23], we create Monte-Carlo realizations of the masses of progenitor halos and the redshifts at which they merge to form a larger halo. These “merger trees” (each branch in the tree represents a halo merging event) reflect the collapse and merging of dark matter halos within a specific cosmology and have been shown to agree fairly well with merger trees extracted from N-body simulations [24]. Each halo at the top level of the hierarchy is assumed to be filled with hot gas, which cools radiatively and collapses to form a gaseous disk. The cooling rate is calculated from the density, metallicity, and temperature of the gas. Cold gas is turned into stars using a simple recipe, depending on the mass of cold gas present and the dynamical time of the disk. Supernovae inject energy into the cold gas and may expell it from the disk and/or halo if this energy is larger than the escape velocity of the system. Chemical evolution is traced assuming a constant yield of metals per unit mass of new stars formed. The spectral energy distribution (SED) of each galaxy is then obtained by assuming an IMF and using stellar population models (e.g. [25]; in the present work we use the updated GISSEL98 models with solar metallicity). When halos merge, the galaxies contained in each progenitor halo retain their separate identities until they either fall to the center of the halo due to dynamical friction and merge with the central galaxy, or until they experience a binding merger with another satellite galaxy orbiting within the same halo. All galaxies are assumed to start out as disks, and major (nearly equal mass) mergers result in the formation of a spheroid. New gas accretion and star formation may later form a new disk, resulting in a variety of bulge-to-disk ratios at late times. This may be used to divide galaxies into rough morphological types, and seems to reproduce observational trends such as the morphology-density relation and color-morphology trend [18,26].

The recipes for star formation, feedback, and chemical evolution contain free parameters, which we set by requiring an average fiducial “Milky Way” galaxy to have an I-band magnitude, cold gas mass, and metallicity as dictated by observations of nearby galaxies. The star formation and feedback processes are some of the most uncertain elements of these models, and indeed of any attempt to model galaxy formation. We have investigated several different combinations of recipes for star formation and supernova feedback (sf/fb), discussed in detail in [16], [17] and [22]. The star formation history for several different scenarios is shown in Figure 1. Note that the three models shown in Figure 1 are for the same SCDM cosmology; the only difference is in the mechanism used to convert cold gas into stars. This illustrates that, unlike in the previous approach of MP96, the star formation history of the Universe is quite sensitive to the assumed astrophysics and not only the cosmology. Here we will discuss results for a single choice of sf/fb recipe, which corresponds to the fiducial “Santa Cruz” model discussed in [16], and is similar to the models of Kauffmann et al. (e.g. [18,30]). We shall elaborate on the effects of changing

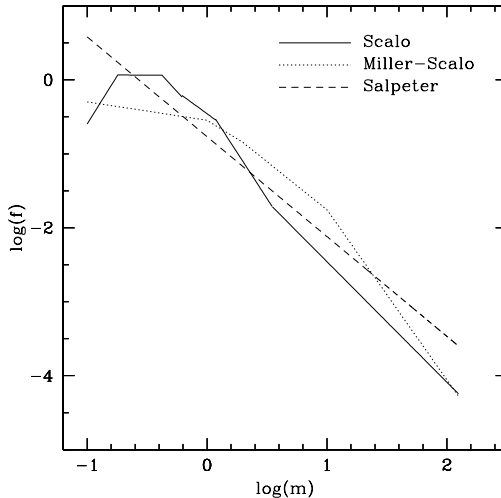


Fig. 2. Stellar initial mass functions (IMFs): Scalo [27], Miller-Scalo [28], and Salpeter [29]; $f(m)dm$ is the mass fraction in stars with mass in the interval $m, m + dm$, where m is in units of M_\odot .

the sf/fb recipes on the EBL and gamma ray absorption in [5] and [6].

In [16], we included dust extinction using the same approach as MP96. As shown in [16], this led to better results for the B-band luminosity function, and improved galaxy colors. Using a similar approach to modelling dust extinction, [30] confirmed these results and demonstrated that in addition the inclusion of dust greatly improves the agreement of the galaxy-galaxy correlation function with observations. The inclusion of dust extinction and the re-radiation of absorbed light at longer wavelengths is of course a crucial ingredient in modeling the EBL. The current dust model, discussed in [15], is an improved version of the one used in MP96, and is very similar to the approach used by Guiderdoni et al. [31]. As in MP96, all of the absorbed starlight is re-radiated by the dust, assuming a three-component blackbody emission spectrum. However, in MP96 the shape of the dust emission spectrum was chosen to match that of the Galaxy, which is inconsistent with the global data for IRAS galaxies. In the current models, the temperatures and relative contributions of the three components are determined by requiring the colors at 12, 25, and 60 μm to match the observed colors of IRAS galaxies [32]. Details will be given in [5].

4 Initial Mass Function

The stellar initial mass function determines the wavelength distribution of starlight produced by a stellar population of a given age, and as such it is an important ingredient in the calculation of the EBL. In MP96 we considered

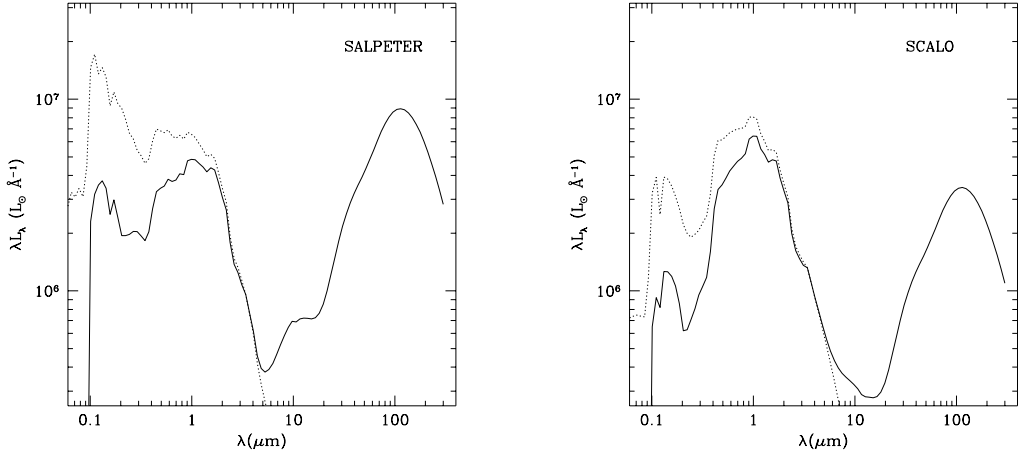


Fig. 3. The spectrum of an average “Milky Way” sized galaxy, assuming a Salpeter (left) or Scalo (right) IMF. The dotted lines show the spectra of starlight without the effects of dust. The solid lines show the spectra with the effects of extinction and emission by dust.

only the Salpeter IMF and steeper power-law IMFs, but here we will discuss results both for the Salpeter IMF and the Scalo IMF (see Figure 2). These are two of the most commonly used IMFs, although recent studies (e.g., [33]) indicate that a better representation of the observed IMF may be a Salpeter-like slope at $M \gtrsim M_\odot$, with a flattening at $M \lesssim M_\odot$. The most important difference between the Salpeter and Scalo IMFs for our present purposes is that if both are normalized to the same total mass of stars, the fraction of high-mass stars is higher with the Salpeter IMF. Since only high-mass stars emit significant amounts of ultraviolet light, this results in much more ultraviolet in the spectrum of a typical galaxy with Salpeter IMF as compared with Scalo IMF, as shown in Figure 3, both without and with inclusion of the effects of dust. Note that the much greater amount of absorbed ultraviolet light with the Salpeter IMF results in much more reradiated infrared light at long wavelengths. Also note that changing the IMF has a relatively small effect on the predictions in the 1-10 μm range.

Previous SAM calculations of properties of local galaxies (e.g. [18,19,16]) assumed a Scalo IMF. However, in [34] and [17], it was shown that a more “top-heavy” IMF (more high-mass stars) such as the Salpeter IMF is favored by observations of UV-bright galaxies at very high redshift (Lyman-break galaxies). In [5], we investigate the effects of using different IMFs (Scalo or Salpeter) on the observable properties of galaxies at $z = 0$. In particular, we calculate the luminosity function at 2000Å, B, R, and K, the corresponding 2000Å-B, B-V, B-I, and B-K colors predicted by our models, and the Tully-Fisher relation in various bands. We find that because the mass-to-light ratio in the longer wavebands (I to K) is significantly higher for the Salpeter IMF, the luminosity of a galaxy with a given velocity dispersion is smaller. This

Table 1

Parameters of Cosmological Models. From left to right, the tabulated quantities are: the age of the universe in Gyr, the Hubble parameter, the matter density, baryon density, density of hot dark matter, density in the form of a cosmological constant in units of the critical density, the slope (or ‘tilt’) of the primordial power spectrum, and the rms mass variance on a scale of $8h^{-1}$ Mpc. The last two columns indicate whether the models are consistent with the observed cluster abundance and the COBE normalization, respectively.

Model	t_0	h	Ω_m	Ω_b	Ω_ν	Ω_Λ	n	σ_8	clusters	COBE
SCDM	13.0	0.50	1.0	0.08	0.0	0.0	1.0	0.67	Y	N
CHDM	13.0	0.50	1.0	0.08	0.2	0.0	1.0	0.65	Y	Y
OCDM	12.7	0.60	0.5	0.056	0.0	0.0	1.0	0.85	Y	Y
LCDM	14.5	0.60	0.4	0.056	0.0	0.6	1.0	0.84	Y	Y

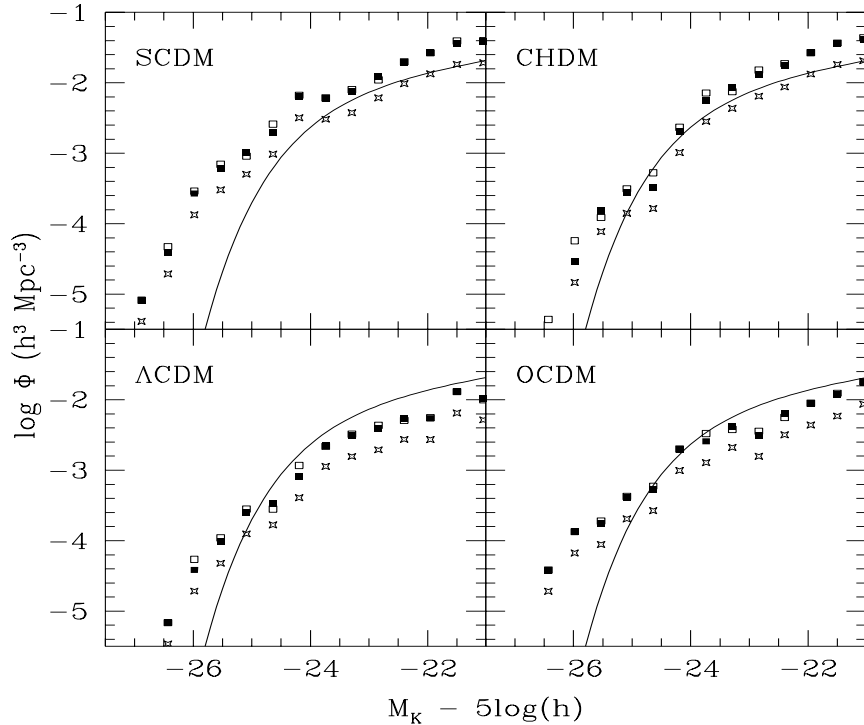


Fig. 4. The predicted K-band luminosity function for the four cosmologies considered here. Open and filled squares indicate the model results with and without dust extinction, respectively, and the star symbols indicate the approximate correction for the inaccuracy of the Press-Schechter method (see text). Solid lines show fits to the recent observational determination of the K-band luminosity function [35].

makes it very difficult to obtain a bright enough Tully-Fisher zero-point in cosmologies with $\Omega_{\text{matter}} = 1$, in which the baryon fraction is low (we assume a fixed value of $\Omega_b h^2 = 0.02$, as suggested by observations [36]; the baryon fraction $f_b \equiv \Omega_b / \Omega_{\text{matter}}$ is therefore higher in low- Ω_{matter} cosmologies). If the

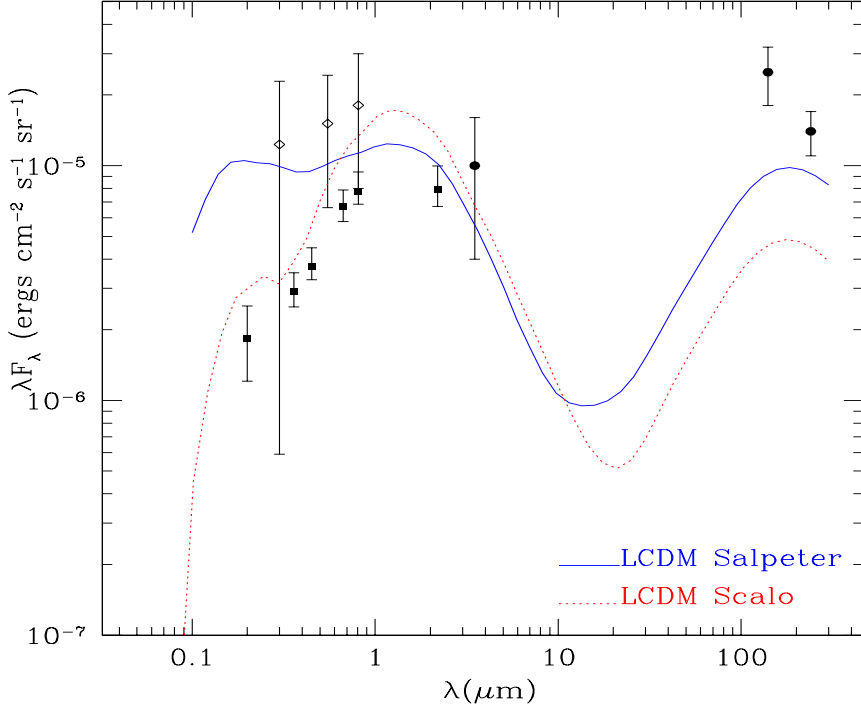


Fig. 5. The $z = 0$ EBL as calculated using SAM models for an LCDM universe assuming both Scalo and Salpeter IMFs. The Salpeter IMF produces more high mass stars, thus more ultraviolet light to be absorbed and re-radiated by dust at $\sim 100 \mu\text{m}$. The filled dots are DIRBE detections of the EBL at 140 and $240 \mu\text{m}$ [37] and $3.5 \mu\text{m}$ [38]. The solid squares are from [39] using HDF galaxy counts, and the open diamonds are from [40], as reported by [41].

mass-to-light ratios predicted by the current generation of stellar population models are accurate and the Salpeter IMF is really representative of typical galaxies, this may suggest that the baryon fraction in bright galaxies must be $0.15 - 0.2$, similar to the value in groups and clusters.

5 Predicted EBL

In [5], we calculate the predicted EBL for several cosmologies and also investigate the effects of the assumed IMF and star formation recipe, and the variations among stellar population models compiled by different groups. Here we can only present a subset of preliminary results. The cosmological models considered are summarized in Table 1. The SCDM model is shown for comparison with other work, but is ruled out by many independent observational considerations. The three remaining models represent currently favored variants of the CDM family of models. The shape and normalization of the luminosity function that we obtain from the SAMs depends on the cosmolog-

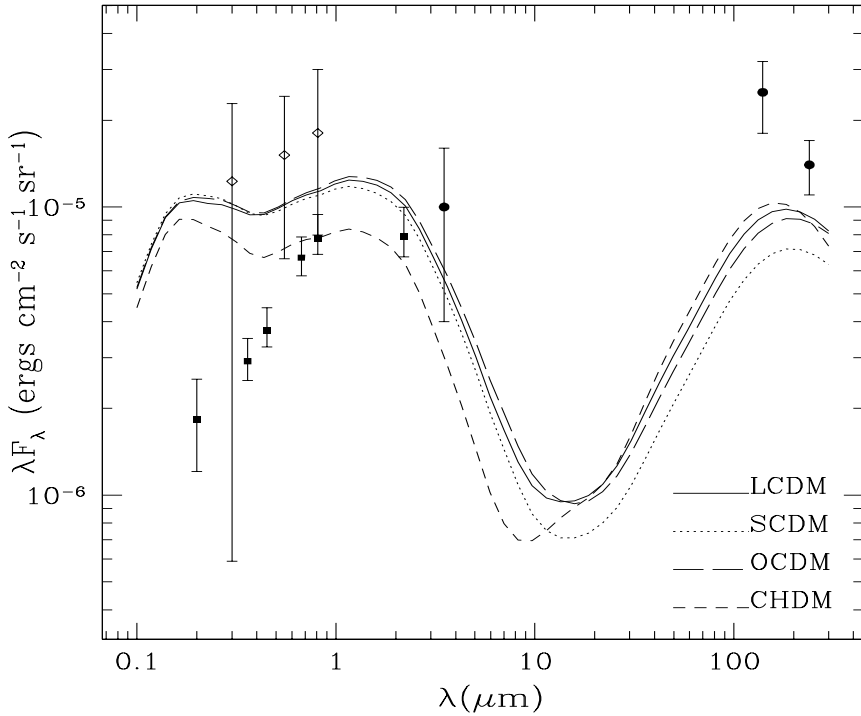


Fig. 6. Predicted extragalactic background light for all four cosmologies considered here (Salpeter IMF). The data points are the same as those in Figure 5. The three models in which galaxy and star formation is relatively early predict similar EBL, while CHDM predicts lower EBL, because galaxies form more recently.

ical model, as shown in Figure 4. The K-band luminosity function shown in the figure is relatively insensitive to dust and the star formation history. To put the models on an equal footing, following a similar logic to the B-band local luminosity function normalization of MP96, we renormalize each model to give the same integrated luminosity in the K-band. The common normalization is obtained by integrating the observed local luminosity function from Ref. [35]. The resulting correction factors range from 0.42 for SCDM to 1.7 for LCDM. Note that this renormalization also sidesteps the known inaccuracy of the Press-Schechter model used to estimate the number density of dark matter halos. The factor of 0.42 for SCDM is consistent with the rule-of-thumb factor of 0.5 determined from comparison with N-body simulations [24,42].

Figure 5 shows the EBL for the LCDM model for the Scalo and Salpeter IMFs. As expected from our previous discussion, the predicted EBL is much higher for the Salpeter IMF at both short and long wavelengths, but the predictions are very similar in the 1-10 μm band that is most relevant for $\sim \text{TeV}$ γ -ray attenuation from relatively nearby sources, in agreement with MP96. Note that both EBL curves are consistent with the lower limits from source counts at ultraviolet, optical, and near-infrared wavelengths (filled symbols), but neither curve is high enough to agree with the new DIRBE EBL detections at 140 and

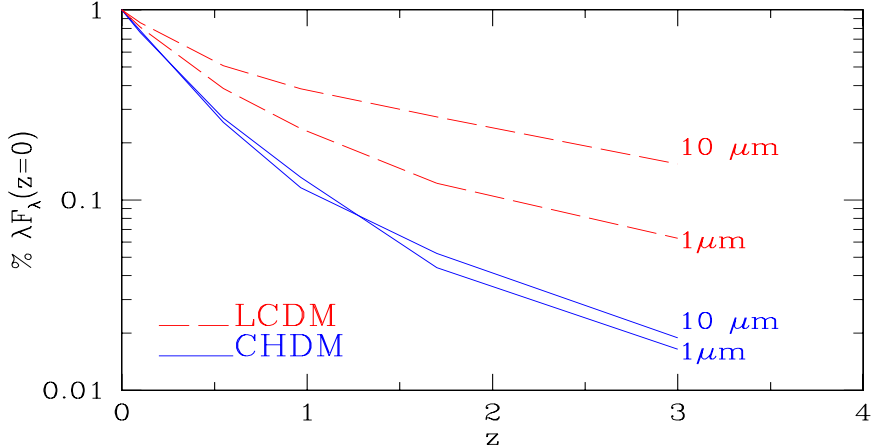


Fig. 7. Evolution of the extragalactic background light. Each curve shows the fraction of the 1 and 10 μm EBL (λF_λ) at the present epoch ($z = 0$) coming from galaxies radiating at redshift $\geq z$. We show the evolution for our CHDM and LCDM models. Due to the later onset of structure formation in the CHDM model relative to LCDM, a much lower fraction of the $z = 0$ EBL comes from galaxies at high-redshift.

240 μm [37].

The remaining results that we present are all for the Salpeter IMF. Figure 6 shows the predicted EBL for the four cosmological models discussed above. Note that the three models in which galaxy and star formation are relatively early predict rather similar EBL, while CHDM predicts generally lower EBL. Figure 7 shows the reason for this in more detail. Only about 10% of the EBL in the 1-10 μm band comes from $z \geq 1$ for the CHDM model, compared to 20-40% for the LCDM model, in which galaxies form considerably earlier. (An alternative way of looking at the evolution of the EBL is given in Figure 8 of [22].) Keep in mind, however, that even in a model with an “early formation” cosmology like LCDM but which assumes less efficient star formation at high redshift (for example, the model with the star formation history indicated by the light solid line in Figure 1), the EBL will show a steeper evolution than that shown in Figure 7 for LCDM. So we expect some degeneracy between cosmology and astrophysics. However, to the extent that the background cosmology may soon be determined by other methods, measurements of the EBL will provide useful constraints on the star formation history of the Universe.

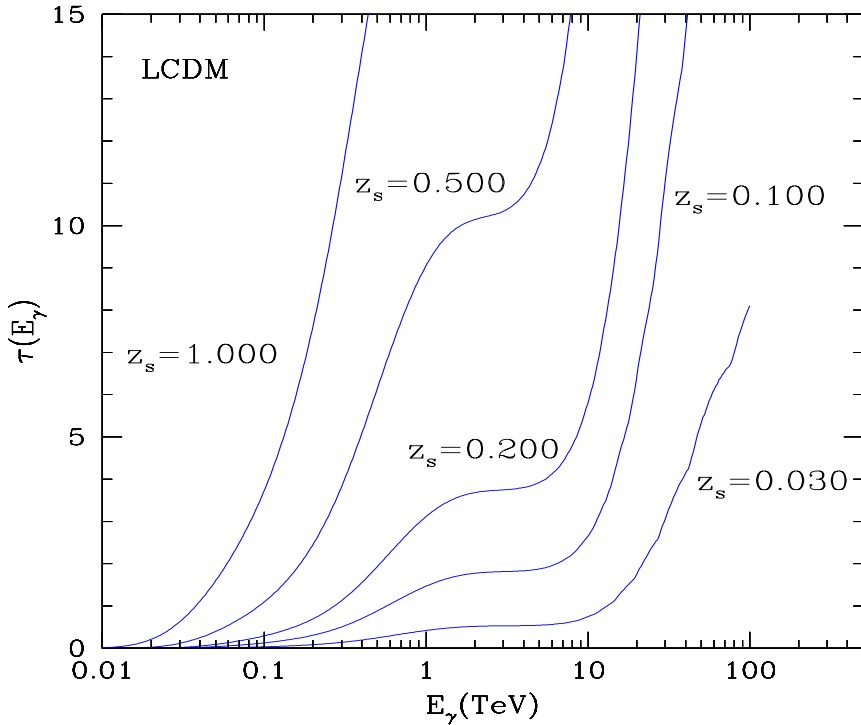


Fig. 8. Optical depth of the universe to γ -rays as a function of γ -ray energy, E_γ , for LCDM with Salpeter IMF. The assumed redshift of the source, z_s , is indicated for each curve.

All of the models fall short of the DIRBE detection at 140 μm by at least a factor of ~ 2.5 . This may be due to a number of effects that we have not yet included in our modeling. Much of the far-infrared and sub-mm light is probably produced by heavily extinguished ultra-luminous starburst galaxies. The phenomenological work of Guiderdoni et al. [31] suggests that the contribution from this population may increase with redshift. Our independent work suggests a physical reason for this: the galaxy interactions that probably trigger these starburst events are more frequent at higher redshift because of the higher density of the Universe, and galaxies are more gas rich so the starburst events may be more dramatic [17]. Observations of nearby starburst galaxies (cf. [43]) suggest that the Galactic/SMC model that we have used here does not provide a good description of dust extinction in actively star forming galaxies. Additional contributions to the far-IR flux that we have not included may come from AGN and from energy that is injected into the gas by supernovae and later radiated at long wavelength. We will include the contribution of starburst galaxies and address these other effects in improved models that we are developing in collaboration with Bruno Guiderdoni and Julien Devriendt. However, we do not expect that this improved treatment will have much effect on the absorption of γ -rays with energies $\lesssim 10$ TeV, which we now discuss briefly.

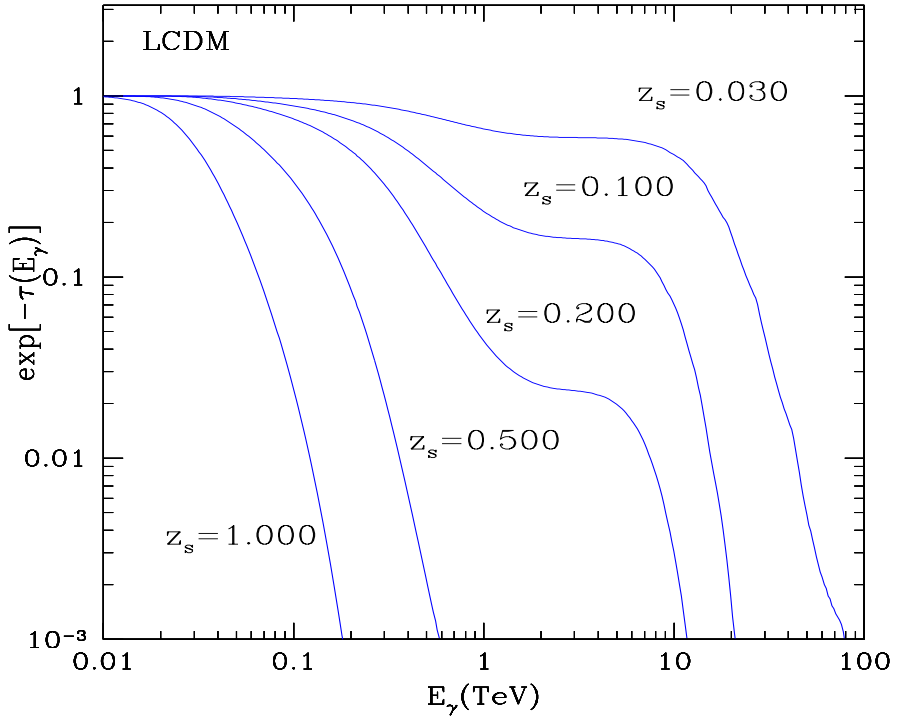


Fig. 9. The attenuation factor, $\exp(-\tau)$ for γ -rays as a function of γ -ray energy for LCDM with Salpeter IMF. The curves are those corresponding to the optical depths $\tau(E_\gamma)$ shown in Figure 8. The value of z_s indicates the assumed source redshift.

6 Attenuation of TeV Gamma Rays

Here we have space to present only the results for one case, LCDM with Salpeter IMF. Figure 8 shows the optical depth of the universe $\tau(E_\gamma)$ as a function of γ -ray energy for varying source redshifts, z_s . The corresponding attenuation factors, $\exp(-\tau)$, are shown in Figure 9. Note that for sources as near as Mrk 421 and 501 ($z = 0.03$), attenuation is predicted to be rather small between 1-10 TeV, with little curvature in the spectrum. Gamma-ray energies $E_\gamma \gtrsim 10$ TeV for local sources, or sources at $z \gtrsim 0.1$ for lower energies, will likely be needed in order to see significant attenuation.

In [6] we will present results for several cosmological models, and discuss dependence on IMF and star formation prescriptions. Bullock et al. [44] discusses the difference in predicted γ -attenuation between Salpeter and Scalo IMF for this same LCDM model. The early universe is much more transparent to 10-100 GeV γ -rays with the Scalo IMF, since the fraction of high-mass stars is lower, and the ultraviolet flux density is correspondingly reduced (cf. [45,6]).

7 Conclusions

- Semi-analytic models (SAMs) of galaxy formation provide a convenient and powerful theoretical framework to determine how input assumptions — e.g., cosmology, star formation history, and IMF — affect the predicted extra-galactic background light (EBL) and the resulting \sim TeV γ -ray attenuation.
- The 1-10 μm EBL and the resulting attenuation of few-TeV γ -rays reflect mainly the history of star formation in the universe, with less attenuation for models such as CHDM in which galaxies form relatively late.
- The EBL at $\lesssim 1 \mu\text{m}$ and $\gtrsim 10 \mu\text{m}$ is significantly affected by the IMF and the modeling of the absorption and reradiation by dust.
- Gamma-ray energies $E_\gamma \gtrsim 10 \text{ TeV}$ and/or sources at $z \gtrsim 0.1$ will probably be needed to provide clear evidence of attenuation due to $\gamma\gamma \rightarrow e^+e^-$.
- Therefore, both space- and ground-based γ -ray telescopes will be required to probe the spectra of AGNs at various redshifts, in order to determine both
 - the unabsorbed spectra, which will help determine how these γ -rays are produced, and
 - the intergalactic absorption, which as we have shown is affected by cosmology, star formation history, IMF, and dust.

Acknowledgments

JRP and JSB were supported by NSF and NASA grants at UCSC, and RSS was University Fellowship from The Hebrew University. JRP thanks Avishai Dekel for hospitality at Hebrew University. Donn MacMinn contributed significantly to an early stage of this work, especially the dust modeling. His life was tragically cut short by a hit-and-run driver as he was bicycling near Chicago on August 30, 1997.

References

- [1] R.J. Gould, G.P. Schréder 1967, Phys. Rev., 155, 1404.
- [2] S.D. Biller, these proceedings.
- [3] F.W. Stecker, these proceedings.
- [4] D. MacMinn, J.R. Primack 1996, Space Science Reviews, 75, 413.
- [5] R.S. Somerville, J.S. Bullock, J.R. Primack, in prep.
- [6] J.S. Bullock, R.S. Somerville, D. MacMinn, J.R. Primack, in prep.

- [7] R.B. Partridge, P.J.E. Peebles 1967, *ApJ*, 148, 377.
- [8] Y. Yoshii, F. Takahara 1988, *ApJ*, 326, 1.
- [9] A. Franceschini, P. Mazzei, G. DeZotti, L. Danese 1994, *ApJ*, 427, 140.
- [10] B. Guiderdoni, B. Rocca-Volmerange 1987, *A&A*, 186, 1.
- [11] F.X. Desert, F. Boulanger, J.L. Puget 1990, *A&A*, 237, 215.
- [12] J.A. Zweerink et al. 1997, *ApJ*, 490, L141.
- [13] F.W. Stecker, O.C. DeJager, M.H. Salamon 1992, *ApJ*, 390, L49; O.C. DeJager, F.W. Stecker, M.H. Salamon 1994, *Nature*, 369, 294.
- [14] Stecker, FW; deJager, OC. 1997, *ApJ*, 476, 712.
- [15] Somerville, R.S. 1997, Ph.D. dissertation, University of California, Santa Cruz.
- [16] R.S. Somerville, J.R. Primack 1998, *MNRAS*, in press (astro-ph/9802268).
- [17] R.S. Somerville, J.R. Primack, S.M. Faber 1998, *MNRAS*, in press (astro-ph/9806228).
- [18] G. Kauffmann, S.D.M. White, B. Guiderdoni 1993, *MNRAS*, 264, 201.
- [19] S. Cole, A. Aragón-Salamanca, C.S. Frenk, J.F. Navarro, S.E. Zepf 1994, *MNRAS*, 271, 781.
- [20] M. Pettini, D.L. King, L.J. Smith, R.W. Hunstead 1998, *ApJ*, 478, 536.
- [21] D. Hughes et al. 1998, *Nature*, 394, 241.
- [22] R.S. Somerville, J.R. Primack 1998, in Proceedings of the Xth Recontre de Blois, June 1998, eds B. Guiderdoni et al. (Editions Frontieres) (astro-ph/9811001).
- [23] R.S. Somerville, T.S. Kolatt 1998, *MNRAS*, in press (astro-ph/9711080).
- [24] R.S. Somerville, G. Lemson, T.S. Kolatt, A. Dekel 1998, *MNRAS*, in press (astro-ph/9807277).
- [25] A.G. Bruzual, S. Charlot 1993, *ApJ*, 405, 538.
- [26] C.M. Baugh, S. Cole, C.S. Frenk 1996, *MNRAS*, 283, 1361.
- [27] J.M. Scalo 1986, *Fund. Cosmic Phys*, 11, 1.
- [28] G. Miller, J.M. Scalo 1979, *ApJS*, 41, 513.
- [29] E. Salpeter 1955, *ApJ*, 121, 61.
- [30] G. Kauffmann, J.M. Colberg, A. Diaferio, S. D.M. White 1998, *MNRAS*, in press (astro-ph/9805283)
- [31] B. Guiderdoni, E. Hivon, F.R. Bouchet, B. Maffei, 1998, *MNRAS*, 295, 877.

- [32] Soifer, B. et al. 1987, *ApJ*, 320, 238.
- [33] J. Scalo 1998, in *Proceedings of the Xth Recontre de Blois*, June 1998, eds B. Guiderdoni et al. (Editions Frontieres) (astro-ph/9811341).
- [34] C.M. Baugh, S. Cole, C.S. Frenk, C.G. Lacey 1998, *ApJ*, 498, 504.
- [35] G.P. Szokoly, M.U. Subbarao, A.J. Connolly, B. Mobasher 1998, *ApJ*, 492, 452.
- [36] D. Tytler, S. Burles, L. Lu, X.-M. Fan, A. Wolfe, B.D. Savage 1999, *AJ*, in press (astro-ph/9810217).
- [37] G. Hauser et al. 1998, *ApJ*, in press (astro-ph/9806167).
- [38] E. Dwek, R.G. Arendt 1998, *ApJL*, in press (astro-ph/9809239).
- [39] L. Pozzetti et al. 1998, *MNRAS* submitted (astro-ph/9803144).
- [40] R.A. Bernstein, W.L. Freedman, B.F. Madore 1998, in prep.
- [41] E. Dwek et al. 1998, *ApJ*, in press (astro-ph/9806129).
- [42] M.A.K. Gross, R. Somerville, J.R. Primack, J. Holtzman, A.A. Klypin 1998, *MNRAS*, 301, 81 (1998).
- [43] Calzetti, D. 1997, *AJ*, 113, 162
- [44] J.S. Bullock, R.S. Somerville, D. MacMinn, J.R. Primack, these proceedings.
- [45] P. Madau, E.S. Phinney 1996, *ApJ*, 456, 124.